Lunar Orbit Design of a Satellite Swarm for Radio Astronomy

Mok, Sung-Hoon; Guo, Jian; Gill, Eberhard; Rajan, Raj Thilak

DOI
10.1109/AERO47225.2020.9172468

Publication date
2020

Document Version
Final published version

Published in
2020 IEEE Aerospace Conference

Lunar Orbit Design of a Satellite Swarm for Radio Astronomy

Sung-Hoon Mok
Faculty of Aerospace Engineering
Delft University of Technology
Delft, The Netherlands
s.mok@tudelft.nl

Jian Guo
Faculty of Aerospace Engineering
Delft University of Technology
Delft, The Netherlands
j.guo@tudelft.nl

Eberhard Gill
Faculty of Aerospace Engineering
Delft University of Technology
Delft, The Netherlands
e.k.a.gill@tudelft.nl

Raj Thilak Rajan
Faculty of EEMCS
Delft University of Technology
Delft, The Netherlands
r.t.rajan@tudelft.nl

***Abstract*—Employing a satellite swarm for radio astronomy has been continuously addressed in the Orbiting Low Frequency ARray (OLFAR) project. A 100 km diameter of aperture array constructed by distributed satellites will be able to provide sky maps of better than 1 arc-minute spatial resolution at 10 MHz. However, an orbit design strategy for the swarm satellites that ensures safe intersatellite distances and relative orbit stability has not yet been developed. In this paper, a new method for OLFAR orbit design is proposed. A deterministic solution is presented based on three algebraic constraints derived here, which represent three orbit design requirements: collision avoidance, maximum baseline rate, and uvw-space coverage. In addition, an idea for observation planning over the mission lifetime is presented.**

TABLE OF CONTENTS

1. INTRODUCTION

In the recent decades, radio astronomy in the frequencies between 30 MHz (10 m wavelength) and 3 GHz has been successfully studied by ground-based radio telescopes. However, space-based observation is considered as the only viable option for producing sky maps with cosmic signals below the 30 MHz since the signals are blocked by the Earth ionosphere [1,2]. Science at this ultra-low wavelength (ULW) regime can provide insights for the study of galactic survey and of exploring our solar system. The most interesting aspect is the study of the very early universe, referred to as dark ages, because the global 21-cm wave absorption signature is expected to peak around 30 MHz [1].

978-1-7821-2734-7/20/$31.00 ©2020 IEEE

Observation below 30 MHz from space was initiated by two US missions: RAE-1 [3] and RAE-2 [4]. In 1968, RAE-1 was launched to the Earth orbit and observed the 0.2-9.2 MHz frequency band. In 1973, RAE-2 was launched to the lunar orbit and mapped the 25 kHz to 13 MHz frequency band. In 1988 and 2000, other space-based array missions, LFSA [5] and ALFA [6], were proposed. Recently, in 2012, a single satellite lunar orbiting mission (DARE) was proposed, operating at 125 km altitude for 2 years of mission period [7]. In 2018, the LCRT mission [8] was proposed to observe the 2-60 MHz frequency band with deployed antennas on the lunar surface. In Europe, together with constructing the largest low-frequency radio telescope LOFAR for 30-250 MHz frequency observation, several space-based array missions have been proposed. Between 2009-2010, two ESA-funded projects, FIRST [9] and DARIS [10], studied passive formation flying missions using arrays synthesis. The knowledge and experience gained were connected to the SURO-LC mission [11]. Since 2010, a new concept for radio astronomy based on a distributed architecture was proposed by the Orbiting Low Frequency ARray for radio astronomy (OLFAR) framework. The OLFAR mission has been jointly studied by several Dutch universities and research institutes. More details on the space-based astronomy missions can be found in [1,2].

Deployment locations and orbits of the satellite swarm are crucial to meet OLFAR system requirements. Several deployment locations have been suggested, including the Earth-Moon Lagrange points, heliocentric orbit, high Earth orbit, and lunar orbit [1,12]. The most promising orbit considered is the lunar orbit since the radio frequency interference (RFI) can be minimized on the far side of the Moon. In [13], two lunar orbits at altitudes of 200 and 3000 km were considered as reference orbits, and their relative orbits were designed to maximize the uvw coverage, by applying numerical optimization. However, the study concluded that the baseline rate requirement (which is 3 m/s) cannot be satisfied in lunar orbit, except at very high altitudes. This issue has been considered as a bottleneck to realize the OLFAR mission in lunar orbit [1,2].

In this paper, a new method for OLFAR orbit design is proposed, which mitigate the baseline rate problem in the low lunar orbit. By confining observation points and controlling along-track offsets, the baseline rate during observation can be minimized. A systematic approach to design reference and relative orbits is proposed. The complexity of the original orbit design problem can be greatly reduced by transforming the system requirements into three simple algebraic equations, which represent collision avoidance requirement, uvw coverage requirement, and baseline rate requirement, respectively. In addition, observation scheduling for a satellite swarm is presented.

The remainder of this paper is outlined as follows. Section 2 introduces OLFAR system requirements and candidates of the deployment location studied so far. Section 3 presents a guideline of determining reference orbit with respect to the system requirements. In Section 4, three algebraic conditions in terms of relative orbit elements are derived. A general scheme for relative orbit design including an observation scenario is also presented. Section 5 concludes the paper with future work planned.

2. OLFAR Requirements and Orbits

OLFAR is a Dutch-funded project initiated in 2010. A team of several universities and research institutes have worked on the project, which aims at employing several or tens (or even hundreds) of satellites that operate together in a distributed system framework, to avoid the single point of failure and to enable operation without a centralized mothership. OLFAR aims at opening up the 0.3-30 MHz for radio astronomy, and its ultimate goal is to provide high-quality sky maps with a ≤ 1 arc-minute of spatial resolution below the 10 MHz frequency. Further details on a concept of operations of OLFAR can be found in two PhD thesis work [12,14] and in [1]. A recent roadmap towards realizing the OLFAR mission was presented in [2]. The study introduced 4 distinct phases to enable a deployment of a satellite swarm in lunar orbit until 2030.

System Requirements

A list of high-level system requirements of OLFAR is summarized in Table 1 [1,2,15]. In this paper, two system requirements are fixed for orbit design; the number of satellites is 50 and the mission lifetime is 2 years. The total observation time for 50 satellites is approximately 480 hours, which is obtained from the cumulative observation time requirement and sensitivity requirement [16].

Table 1. System requirements in OLFAR.

Number of satellites	≥ 10
Observation frequency	0.3-30 MHz
Observation wavelength	1000-10 m
Instantaneous bandwidth	≥ 1 MHz
Maximum baseline length	100 km
Spatial resolution	1 arc-minute at 10 MHz
Snapshot integration time	1-1000 s

Two important system requirements for orbit design are the maximum baseline length and the snapshot integration time. First, maximum baseline lengths are determined by the synthesized aperture diameter for radio astronomy missions. In OLFAR, a swarm orbit should allow satellites to fill (i.e., reach) uvw points within a sphere, whose diameter is 100 km. Figure 1 gives an example of the relationship between satellite positions and uv points, assuming 10 satellites. Second, the snapshot integration time requirement generates a maximum baseline rate requirement. The requirement can be understood as a stability requirement of relative orbit. When observation takes place, baseline rates (i.e., range rates) between satellites should not exceed a maximum baseline rate limit, which is 3 m/s in OLFAR.

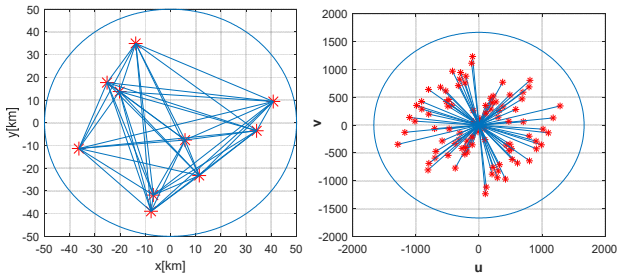

Figure 1. (Left) Satellite positions and baseline vectors, and (right) corresponding uv points.

Candidates for Deployment Location and Swarm Orbit

Several deployment locations for a satellite swarm have been studied in OLFAR. The following conditions have been considered as major factors for deployment location selection: low RFI during observation, maximum possible downlink data-rate, relative orbit stability [1]. Deployment location candidates include the Earth-Moon Lagrange points (L2/L4/L5), high Earth orbit, lunar surface, lunar orbit, and heliocentric orbit. Each deployment location has pros and cons; however, lunar orbit is considered as the most promising orbit for radio astronomy due to the existence of the radio quiet zone on the far side of the Moon, and the shortest downlink distance between the swarm and the Earth.

However, a bottleneck of lunar orbit operations is the baseline rate requirement. Dekens et al. [13] conducted case studies with two reference orbits at 200 and 3000 km altitudes in lunar orbit. The study found that highest baseline rates at the 200 and 3000 km altitudes are 116 and 30 m/s, respectively, which are 10 times or more than the maximum baseline rate requirement. In this paper, we propose a relative orbit design method to alleviate the baseline rate problem, but first a design for the reference orbit is presented in the next section.

3. Reference Orbit Design

A reference orbit literally means an orbit that serves as a reference for satellite swarm orbits. Either virtual satellite or real satellite can be present on the reference orbit. Reference orbit design aims to determine six orbit elements (OEs):

$$\boldsymbol{\alpha} = [a \;\; M \;\; e \;\; \omega \;\; i \;\; \Omega]^T \quad (1)$$

where a is the semi-major axis (SMA), M is the mean anomaly, e is the eccentricity, ω is the argument of perigee (AOP), i is the inclination, and Ω is the right ascension of ascending node (RAAN), respectively. Among the six OEs, only the three elements whose mean values are nearly constant during the mission lifetime (against the lunar gravitational perturbations) are considered as design variables here: SMA, eccentricity, and inclination.

There are two system requirements that drive the reference orbit design: a total observation time and a uvw coverage. A trade-off study that illustrates an impact of changes in a, e, and i on the system requirements is introduced in the following.

Trade-off Study

Total Observation Time—is the summation of observation durations over the mission lifetime. Two conditions should hold for effective observation in OLFAR. First, a satellite should be within a given Earth radio eclipse region to take an advantage of low RFI. Second, swarm satellites should satisfy the baseline rate requirement during observation. Unfortunately, the two conditions are in trade-off, with respect to the SMA. In other words, we cannot increase the eclipse fraction and the minimum baseline rate fraction at the same time. For example, the eclipse fraction increases with lower SMA since the satellite approaches closer to the Moon and is increasingly shielded by the Moon against RFI emitted from the Earth. However, baseline rates between the swarm satellites are inversely proportional to the SMA since a velocity of the reference orbit increases.

Meanwhile, impacts of an eccentricity change on the two conditions can be negligible. Although the eclipse fraction becomes irregular with higher eccentricity, a mean eclipse fraction does not change significantly [16]. Lastly, larger inclination makes the mean eclipse fraction smaller, while its impact on the minimum baseline rate fraction is negligible (which mainly depends on the SMA).

UVW Coverage—A continuous change in relative motions between the swarm satellites is crucial to fill out the large uvw sphere of 100 km of diameter. Relative orbits can vary either actively (by orbit maneuvering) or passively (by orbit perturbations). However, considering the limited amount of propellant, exploiting the natural orbit perturbations as much as possible is desirable in OLFAR. A drift motion between two satellites can be described by three drift motions: an along-track drift due to a SMA difference, an in-plane relative drift due to AOP and RAAN drifts, and an out-of-plane relative drift due to an inclination difference.

First, we neglect the along-track drift in our study since SMAs of the satellites are assumed to be the same for a safety purpose, except the certain period of time during reconfiguration. Second, the in-plane drift is mainly caused by the J2 term (in the lunar gravitational model) and it is the most important drift motion for a uvw points diversification. The higher rate of drift enables faster filling of the uvw sphere. More details on the in-plane drift motion (represented by a relative eccentricity vector drift) can be found in the next section. Third and last, inclination differences between the satellites causes a drift in their RAANs. However, the resulting out-of-plane drift motion is minor compared to the in-plane drift motion.

Summary—Table 2 summarizes the trade-off study results. The symbols ▲ indicates that the impact of the certain orbit element change on the system requirement is positive.

Table 2. Trade-off in reference orbit selection.

Requirements		Higher SMA	Higher Eccentricity	Higher Inclination
Total observation time	Mean eclipse fraction	▼	-*	▼
	Minimum baseline rate fraction	▲**		-
UVW coverage	In-plane drift	▼***	▼	▼
	Out-of-plane drift	▼	▼	▲

*Although their mean values are not affected much, less eccentricity is desirable for a consistent mission operations.
**A duty cycle with respect to the baseline rate requirement (3 m/s) varies 2.5% at 270 km altitude to 3.9% at 1000 km altitude to 6.6% at 2000 km altitude, focusing on the relative motion in the cross-track direction. It is the worst-case result when the maximum cross-track distance is 50 km (which corresponds to the edge of the uvw sphere).
***To allow complete circular in-plane drift in two years, an orbital altitude should be lower than 680 km, assuming equatorial orbits.

Reference Orbit Candidates

This paper does not strictly define the reference orbit, but configures a boundary in terms of the orbit elements. First, a reference altitude is confined in $h \in [250, 700]$ km, where the minimum value is driven by the baseline rate requirement and the maximum value is driven by the in-plane drift analysis. Second, an eccentricity e is set to zero, which results in circular orbit. Third, an inclination angle is defined in the range $i \in [0, 45]^o$, where the maximum value is driven by the mean eclipse fraction analysis.

4. Relative Orbit Design

A relative orbit describes a relative motion of one satellite with respect to some other (usually reference) satellite's orbit. It can be represented by either the Hill Cartesian coordinate frame, arithmetic OE differences, or the relative orbital elements (ROEs). In this paper, the ROEs and the Hill Cartesian coordinate frame are mainly adopted to describe the relative motion.

Relative Orbit Elements

Definition—Applying the ROEs in low Earth orbit (LEO) was initially proposed for the precursor formation flying

mission named TanDEM-X [17,18]. The ROE six parameters are defined by

$$\delta\boldsymbol{\alpha} = [\delta a \quad \delta\lambda \quad \delta\mathbf{e}^T \quad \delta\mathbf{i}^T]^T \in \mathbb{R}^{6\times 1} \tag{2}$$

where $\delta\mathbf{e} = [\delta e_x \;\; \delta e_y]^T$ and $\delta\mathbf{i} = [\delta i_x \;\; \delta i_y]^T$ are the relative eccentricity vector and relative inclination vector, respectively. Note that the relative SMA $\delta a = (a - a_c)/a_c$ is a dimensionless component. The first four parameters represent the in-plane relative motion, whilst the last two represent the out-of-plane relative motion. The relative mean longitude $\delta\lambda$ is defined by

$$\delta\lambda = \delta u + \delta\Omega\cos i_c \tag{3}$$

where $u = \omega + M$ is the mean argument of latitude and i_c is the chief orbit inclination. Moreover, $\delta\mathbf{e}$ and $\delta\mathbf{i}$ can be also described in the polar coordinate as

$$\delta\mathbf{e} = \mathbf{e} - \mathbf{e}_c = e\begin{bmatrix}\cos\omega\\ \sin\omega\end{bmatrix} - e_c\begin{bmatrix}\cos\omega_c\\ \sin\omega_c\end{bmatrix} = \delta e\begin{bmatrix}\cos\phi\\ \sin\phi\end{bmatrix} \tag{4}$$

$$\delta\mathbf{i} = \delta i\begin{bmatrix}\cos\theta\\ \sin\theta\end{bmatrix} \tag{5}$$

where ϕ and θ are the argument of latitudes of the relative perigee and of the relative ascending node, respectively.

Transformation into the Hill Frame—Assuming that the reference orbit is circular, and the swarm orbits are close enough to the reference orbit, the ROE parameters can be converted to the Hill frame components by [18]

$$\frac{1}{a_c}\mathbf{r} = \frac{1}{a_c}\begin{bmatrix}x\\ y\\ z\end{bmatrix} = \begin{bmatrix}-\delta e\cos(u-\phi)\\ \delta\lambda + 2\delta e\sin(u-\phi)\\ \delta i\sin(u-\theta)\end{bmatrix} \tag{6}$$

$$\frac{1}{v_c}\dot{\mathbf{r}} = \frac{1}{v_c}\begin{bmatrix}\dot{x}\\ \dot{y}\\ \dot{z}\end{bmatrix} = \begin{bmatrix}\delta e\sin(u-\phi)\\ 2\delta e\cos(u-\phi)\\ \delta i\cos(u-\theta)\end{bmatrix} \tag{7}$$

where $\mathbf{r} = [x \;\; y \;\; z]^T$ is the relative position vector consisting of radial, along-track, and cross-track components and $\mathbf{v} = [\dot{x} \;\; \dot{y} \;\; \dot{z}]^T$ is the relative velocity vector, and $v_c = a_c n_c$. Note that the relative orbit geometry (or shape) is determined by the four parameters: two lengths of the relative vectors, δe and δi, and their associated phase angles, ϕ and θ.

Relative Orbit Conditions to Satisfy the System Requirements
A relative orbit shall be designed according to the relevant system requirements. In the following subsections, three algebraic conditions for these three system requirements are derived.

Collision Avoidance Condition—A collision between satellites shall be avoided. A certain intersatellite distance should be guaranteed during a whole mission lifetime. However, it is cumbersome to check all the distances between the pairs of the satellites in every second. Propagating the orbits as well as checking the intersatellite distances requires tremendous computation time if the number of satellites is large, and the mission lifetime is long.

A systematic condition to ensure the safety for swarm satellites was suggested in [19]. The following equation (Eq. (20) in [19]) describes a condition for guarantying a minimum safe distance ε in the in-plane motion:

$$a_c\left|\delta\lambda_{jk}\right| = a_c\left|\delta\lambda_k - \delta\lambda_j\right| \le f(a_c, \delta e_{jk}, \varepsilon), \quad \forall\, j \ne k \tag{8}$$

$$f(a_c, \delta e, \varepsilon) = \begin{cases}\sqrt{3(a_c^2\delta e^2 - \varepsilon^2)}, & if \quad \varepsilon \le a_c\delta e < 2\varepsilon\\ 2a_c\delta e - \varepsilon, & if \quad a_c\delta e \ge 2\varepsilon\end{cases} \tag{9}$$

where $\delta\lambda_{jk} = \delta\lambda_k - \delta\lambda_j$ and $\delta e_{jk} = \left\|\delta\mathbf{e}_k - \delta\mathbf{e}_j\right\|$ while j and k denote satellite ID. In Eq. (8) we can see that the controlled $\left|\delta\lambda_{ij}\right|$ can guarantee collision avoidance. Eq. (9) can be simplified when the minimum separation between the satellites $a_c\delta e_{ij,\min}$ is set larger than 2ε, which is the assumption we make in this paper. For example, suppose that the minimum safe distance ε is 500 m and $a_c\delta e_{ij,\min}$ is larger than 1 km, then we only need to check whether $\left|\delta\lambda_{ij}\right|$ is smaller than $2a_c\delta e - \varepsilon$ for collision avoidance such that:

$$a_c\left|\delta\lambda_{jk}\right| \le 2a_c\delta e_{jk} - \varepsilon, \quad \forall\, j \ne k. \tag{10}$$

Minimum Baseline Rate Condition—A swarm-to-earth downlink data volume can be reduced by applying a distributed correlation framework, explained in [1]. In addition, a snapshot integration technique can be used for further data volume reduction. However, this imposes a new requirement that the baseline rates between the satellites should be kept minimum during observation period. The baseline rate $\delta\dot{r}$ means the rate of the change of the distance between the satellites:

$$\delta\dot{r} = \frac{(\mathbf{r} - \mathbf{r}_c)\cdot(\dot{\mathbf{r}} - \dot{\mathbf{r}}_c)}{\left\|\mathbf{r} - \mathbf{r}_c\right\|}. \tag{11}$$

Integrating Eqs. (6) and (7) into Eq. (11), the baseline rate can be described by

$$\delta\dot{r} = \frac{x\dot{x} + y\dot{y} + z\dot{z}}{\sqrt{x^2 + y^2 + z^2}} \tag{12}$$

and we can divide the zero-baseline rate condition such that

$$\delta\dot{r} = 0, \qquad when \;\; \delta\dot{r}_{xy} = 0 \;\; and \;\; \delta\dot{r}_z = 0, \;\; where \tag{13}$$

$$\delta\dot{r}_z = \dot{z} \;\; and \tag{14}$$

$$\delta\dot{r}_{xy} = \frac{x\dot{x} + y\dot{y}}{\sqrt{x^2 + y^2}}. \tag{15}$$

First, in the out-of-plane motion, we can find two solutions that yield $\delta\dot{r}_z = 0$. One is $\delta i = 0$, but it confines the satellites

orbits to coplanar orbits, which prevents the swarm from obtaining measurements in out-of-plane direction (z-axis). The other solution is

$$u_{\min,z} = \theta + \frac{\pi}{2} \; or \; \theta + \frac{3}{2}\pi \tag{16}$$

and it corresponds to the z-axis component of the satellite position at $z = a_c \delta i$ or $z = -a_c \delta i$ from Eq. (6). Second, in the in-plane motion, the $\delta \dot{r}_{xy} = 0$ condition is equivalent to the following condition:

$$\frac{1}{a_c v_c}(x\dot{x} + y\dot{y}) = (\delta\lambda + \frac{3}{2}\delta e \sin(u-\phi))\delta e \cos(u-\phi) = 0, \tag{17}$$

which offers three solutions, while the meaningful solution is

$$\delta\lambda_{\min} = -\frac{3}{2}\delta e \sin(u-\phi). \tag{18}$$

The above equation describes the along-track offset condition for eliminating the baseline rate in the XY plane. Note that Eq. (18) is applicable to all u and ϕ, unlike Eq. (16) where u was restricted to the specific locations. Meanwhile, $\delta\lambda$ can be efficiently controlled by exploiting the drift caused by the SMA difference, δa, which can be expressed by

$$\delta\lambda = \delta\lambda_0 - \frac{3}{2}(u - u_0)\delta a \cdot t \tag{19}$$

where t is the time and $\delta\lambda_0 = \delta\lambda(t_0)$ is the initial relative mean longitude.

An interval of mean argument of latitude $\mathbf{u}_{obs}$ centered at $u_{\min}$ for $\delta\dot{r} \le \delta\dot{r}_{\max}$ can be found, where $\delta\dot{r}_{\max}$ means the maximum baseline rate requirement. The interval can be expressed by $\mathbf{u}_{obs} = [u_{\min} - \Delta u_{obs},\ u_{\min} + \Delta u_{obs}]$ whose length is $2\Delta u_{obs}$ that can be related to the observation duration and the duty cycle. The solution can be found by applying linearization, and for brevity, only the final result for $\Delta u_{obs,z}$ is stated below:

$$\Delta u_{obs,z} = \frac{\delta\dot{r}_{\max,z}}{v_c \delta i}. \tag{20}$$

For example, if $a_c = 2418$ km (i.e., 680 km altitude) and $\delta i = 50$ km$/a_c$ while $\delta\dot{r}_{\max,z} = 3$ m/s, then v_c becomes 1.42 km/s and the length of the interval $\mathbf{u}_{obs,z}$ which is $2\Delta u_{obs,z}$ becomes 11.7 degrees, which is equivalent to the observation duration of 11.6 minutes per orbit.

The trajectory in the Hill frame with $\delta\lambda_{\min}$ in Eq. (18) and $u_{\min}$ in Eq. (16) can be easily obtained. The following Cartesian components describe potential observation points:

$$x_{\min} / a_c = -\delta e \cos(u_{\min} - \phi) \tag{21}$$

$$y_{\min} / a_c = \frac{1}{2}\delta e \sin(u_{\min} - \phi) \tag{22}$$

$$z_{\min} / a_c = \pm\delta i. \tag{23}$$

Note that an ellipse of the major axis length of $a_c \delta e$ along the x-axis and of the minor axis length of $a_c \delta e / 2$ along the y-axis will be drawn in the XY plane. The z-axis component will be fixed to the extreme points. Although $u_{\min}$ is fixed, the whole points along the trajectory can be expected to be observed, exploiting drift of relative eccentricity vector, $\dot{\phi}$.

Figure 2 illustrates the observation trajectories in the XY plane. The example was drawn under the following conditions: $a_c \delta e = 60$km and $a_c \delta i = 20$km. In the figure, another observation trajectory is also illustrated, which describes the $(x_{\min}, y_{\min}, z_{\min})$ in the inertial frame. It should be noted that the uvw sphere is defined in the inertial frame such that eventually the uvw points in the inertial frame are used to validate the system requirements like the uvw coverage requirement. One more remark is that there is a phase lag in the inertial $(x_{\min}, y_{\min}, z_{\min})$ components compared to the Hill frame components, and this is due to RAAN drift.

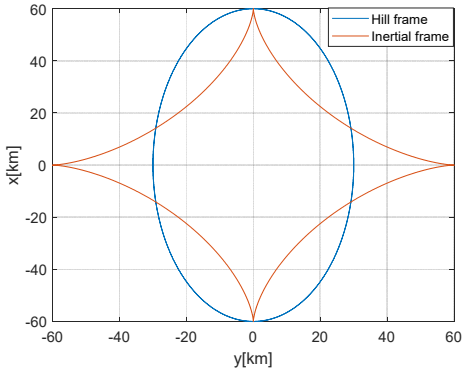

Figure 2. Expected observation points in the Hill (non-inertial) frame and the inertial frame.

UVW Coverage Condition—To complete one circular drift along the observation trajectory in the inertial frame in the given mission period, the following condition should be met:

$$(\dot{\phi} + \dot{\Omega})T \ge 2\pi \tag{24}$$

where

$$\dot{\phi} = \frac{3J_2\mu^{1/2}R^2}{4a^{7/2}(1-e^2)^2}(5\cos^2 i - 1) + \frac{3kn_3^2 a^{3/2}}{8\mu^{1/2}\sqrt{1-e^2}}[(5\cos^2 i - 1 + e^2) + 5(1 - e^2 - \cos^2 i)\cos 2\omega] \tag{25}$$

$$\dot{\Omega} = -\frac{3J_2\mu^{1/2}R^2}{2a^{7/2}(1-e^2)^2}\cos i + \frac{3kn_3^2 a^{3/2}}{8\mu^{1/2}\sqrt{1-e^2}} \times (5e^2\cos 2\omega - 3e^2 - 2)\cos i \tag{26}$$

where T is the mission period (2 years). Details of parameter definitions and equations can be found in [20]. The first and second term describes the drift terms caused by two major perturbations: the J2 perturbation and the 3rd-body gravity perturbation. It is noteworthy that $\dot{\phi} = -2\dot{\Omega}$ when $i_c = 0$. With the altitudes of $h_c = [1200,1000,680,300]$ km, the drift sizes $(\dot{\phi} + \dot{\Omega})T$ become $[180,270,360,540]^o$, assuming $i_c = 0$.

The out-of-plane relative drift motion can be also exploited to diversify the uvw points, although its drift rate is smaller than the in-plane drift rate. The drift motion can be represented by the change in the relative inclination vector. The vertical component of $\delta\dot{\mathbf{i}}$, which is $\delta\dot{i}_y$, presents when $\Delta i \neq 0^o$ such that:

$$\begin{aligned}\delta\dot{i}_y &= (\dot{\Omega} - \dot{\Omega}_c)\sin i_c \\ &\approx -\alpha \sin^2 i_c \cdot \Delta i\end{aligned} \tag{27}$$

where

$$\alpha = -\frac{3J_2\mu_M^{1/2}R_M^2}{2a^{7/2}} + \frac{3kn_3^2a^{3/2}}{8\mu_M^{1/2}\sqrt{1-e^2}}(5e^2\cos 2\omega - 3e^2 - 2) < 0. \tag{28}$$

Again, the first and second term describes the drift motions induced by the J2 term and 3rd-body gravity, respectively. Note that there is no out-of-plane drift when $i_c = 0$.

Relative Orbit Design Method

Observation Scenario—In this subsection, a general idea of observation is introduced. As mentioned earlier, observation is only meaningful when the two conditions are met: the satellites are on the far side of the Moon, and their baseline rates meet the requirement. Figure 3 depicts the change of the eclipse periods in terms of u over 1 month when $h_c = 680$km. It can be seen that the observations occur near to $u_{\min}$. There are two observation periods separated by approximately quarter month. A duty cycle in this example (the ratio of the observation periods over 1 month) is approximately 50 %.

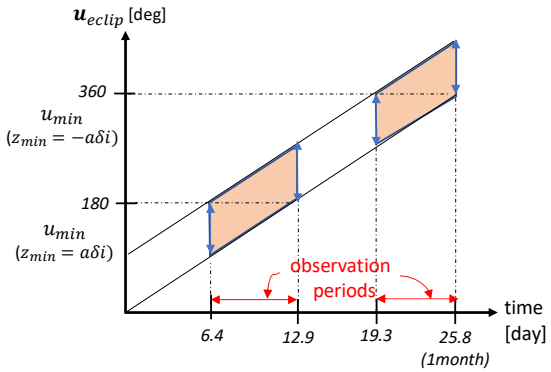

Figure 3. A plot illustrating the observation (eclipse) periods for a 1-month duration.

Figure 4 describes the observation points in the Hill frame for two months. There are in total four observation periods. For each month, the observations take place at the opposite sides of the blue-colored ellipse. This is due to the 180° difference between $u_{\min}$ in Eq. (16). Figure 5 shows instantaneous trajectories at the orbits where observations were performed. It can be seen that the relative orbits are shifted along the y-axis due to the change in $\Delta\delta\lambda_{\min}$ in Eq. (18) according to the change in ϕ. However, the geometries of the relative orbits are the same since it only depends on δe, not ϕ. Again, the conditions of $a_c\delta e = 60$km and $a_c\delta i = 20$km were assumed in this example.

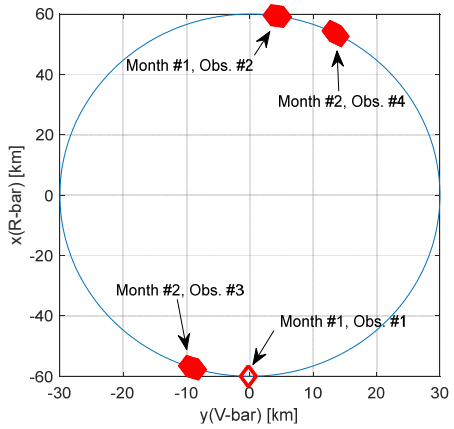

Figure 4. The plot shows the observation points in two months in the XY plane.

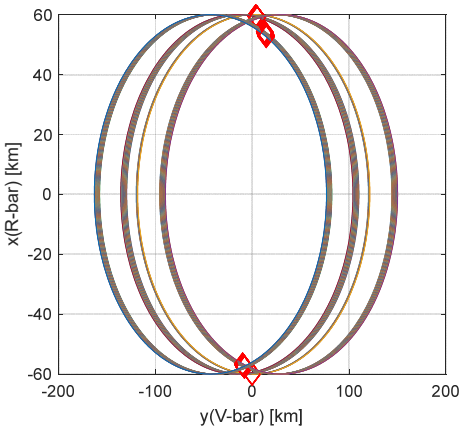

Figure 5. A set of instantaneous trajectories on which the observations were performed.

General Orbit Design Strategy—Referring to the algebraic conditions derived in Eqs. (10), (18), and (24), relative orbits for OLFAR can be efficiently designed. However, before proceeding further, the uvw coverage condition should be further detailed due to the temporal/spatial gaps between the observations, depicted in Figures 3 and 4.

A simple but effective strategy to fill out the gaps by relative orbit design is illustrated in Figure 6. The figure depicts two

monthly observations separated by (approximately) half of the mission lifetime. Starting at $t = t_0$, it can be seen that there are two observation points for one month marked as 1A and 1B in the inner sector. These are analogous to Figure 4. Now suppose that one satellite is added whose relative eccentricity phase angle ϕ differs by 180 degrees to the existing satellite. Then, at the same period of time, the measurements at the opposite side of the ellipse can be obtained, marked as 2A and 2B in the inner sector. However, there still exist the observation gaps since $u_{\min}$ is fixed, and these cannot be covered in the same month. However, the gaps can be filled out after the half circular in-plane drift motion, i.e., after Δt that satisfies $(\dot{\phi} + \dot{\Omega})\Delta t = \pi$. By setting $\Delta t = T/2$, the new measurements at the observation gaps will be starting to be collected from $t = t_0 + T/2$.

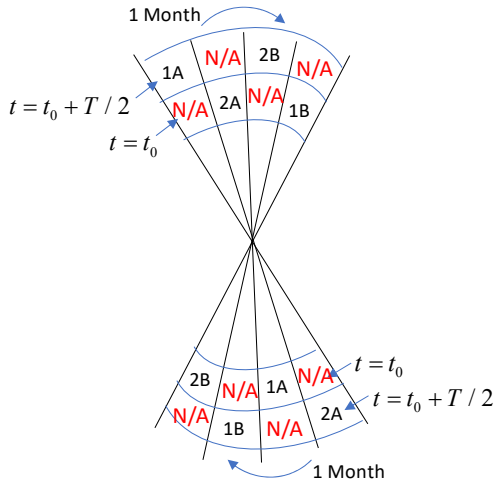

Figure 6. A proposed observation scenario for 2 months.

The last problem for relative orbit design is to optimally assign the satellites in the RZ plane to maximize the uvw coverage. Here, 'R' stands for the radial axis, which is defined by a vector from the reference satellite to a satellite position vector projected onto the XY plane. Design variables of the problem are $\delta e_k(t_0)$, $\delta i_k(t_0)$, $\phi_k(t_0) \in \{0, 180\}^o$, assuming $\theta_k = 90^o$. Hence, the number of the unknown variables is in total $3N$, which is 150 in case of 50 satellites. There exists one constraint in δe_k selection from the safety condition $a_c \left|\delta\lambda_{jk}\right| \le 2a_c\delta e_{jk} - \varepsilon$ from Eq. (10). Combining $\delta\lambda_{\min} = -3/2\delta e\sin(u-\phi)$ in Eq. (18), the safety condition can be converted into $a_c\delta e_{jk} \ge 5/4\varepsilon$. The new safety condition only requires checking whether the maximum relative eccentricity difference δe_{jk} is greater than $5\varepsilon/4a_c$. For example, if the intersatellite distance requirement ε is 500 m, $a_c\delta e_{\min}$ should be greater than 625 m.

However, despite huge complexity reduction from the original orbit design problem, the optimal assignment problem is yet complicated due to the large number of unknowns. Currently, we have been investigating both analytical method (sub-optimal) and numerical method to solve the assignment problem.

5. Conclusions and Future Work

In this paper, an orbit design strategy for the OLFAR mission was proposed. The reference orbit candidates were proposed, in terms of the three orbit elements (SMA, eccentricity, and inclination). For relative orbit design, the three algebraic conditions were derived that can be easily accommodated into the design process. Particularly, the relative orbit constraint for the minimum baseline rate was proposed for the first time here, which eliminates the baseline rate by adjusting the along-track offset. In addition, the mission operation scenario for observation was suggested, which can be useful for mission planning and scheduling of OLFAR.

There are four tasks which we aim to achieve in our ongoing research. First, an optimal configuration to maximize the uvw coverage will be searched. Second, to validate the proposed swarm orbit design, a numerical simulation of long-term orbit propagation based on sophisticated perturbation models will be performed. Third, a delta-v (propellant) cost for the reconfiguration and formation-keeping maneuvers will be analyzed. Last, an end-to-end test for integrated software consisting of proposed swarm orbit, guidance, and control methods, will be conducted.

Acknowledgements

This work was supported by the Dutch-PIPP (Partnerships for Space Instruments & Applications Preparatory Programme), funded by NWO (Netherlands Organisation for Scientific Research) and NSO (Netherlands Space Office).

References

[1] R.T. Rajan, A.-J. Boonstra, M. Bentum, M. Klein-Wolt, F. Belien, M. Arts, N. Saks, A.-J. van der Veen, "Space-based aperture array for ultra-long wavelength radio astronomy," *Experimental Astronomy*, vol. 41, no. 1, pp. 271-306, 2016.

[2] M. Bentum, M.K. Verma, R.T. Rajan, A.-J. Boonstra, C. J.M. Verhoeven, E.K.A. Gill, A.J. Veen, H. Falcke, M. Kelein-Wolt, B. Monna, S. Engelen, J. Rotteveel, L.L. Gurvits, A roadmap towards a space-based radio telescope for ultra-low frequency radio astronomy," *Advances in Space Research*, 2019.

[3] R. Weber, J. Alexander, R. Stone, "The radio astronomy explorer satellite, a low-frequency observatory, *Radio Science*, vol. 6, no. 12, 1971, pp. 1085-1097.

[4] J. Alexander, M. Kaiser, J. Novaco, F. Grena, R. Weber, "Scientific instrumentation of the Radio-Astronomy-Explorer-2 satellite," *NASA STI/Recon Technology Report* N 75, 1974.

[5] K. Weiler, K. Johnston, R. Simon, B. Dennison, W. Erickson, M. Kaiser, H. Cane, M. Desch, "A low frequency radio array for space," *Astronomy and Astrophysics*, vol. 195, pp. 372-379, 1988.

[6] D. Jones, R. Allen, J. Basart, T. Bastian, W. Blume, J.-L. Bougeret, B. Dennison, M. Desch, K. Dwarakanath, W. Erickson, "The ALFA medium explorer mission," *Advances in Space Research*, vol. 26, no. 4, pp. 743-746, 2000.

[7] A.L. Genova, F.Y. Yang, A.D. Perez, K.F. Galal, N.T. Faber, S. Mitchell, B. Landin, A. Datta, J.O. Burns, "Trajectory design from GTO to lunar equatorial orbit for the dark ages radio explorer (DARE) spacecraft," in *AAS/AIAA Space Flight Mechanics Meeting*, Williamsburg, VA, US, Jan. 2015. AAS-15-456.

[8] S. Bandyopadhyay, J. Lazio, A. Stoica, P. Goldsmith, B. Blair, M. Quadrelli, J.-P. Croix, A. Rahmani, "Conceptual ideas for radio telescope on the far side of the Moon," *IEEE Aerospace Conference*, Big Sky, MT, US, March 2018.

[9] J.E.S. Bergman, R.J. Blott, A.B. Forbes, D.A. Humphreys, D.W. Robinson, C. Stavrinidis, "FIRST explorer – An innovative low-cost passive formation-flying system," 2009. arXiv:0911.0991

[10] N. Saks, A.-J. Boonstra, R.T. Rajan, M. Bentum, F. Belien, K. Klooster, "DARIS, A fleet of passive formation flying small satellites for low frequency radio astronomy," In *Small Satellite Systems and Services (4S) Symposium*, Madeira, Portugal, June 2010.

[11] W. Baan, "SURO-LC: A space-based ultra-long wavelength radio observatory," In *Meeting from Antikythera to the Square Kilometre Array*, Kerastari, Greece, June 2012.

[12] S. Engelen, *Swarm Satellites: Design, Characteristics and Applications*, Ph.D. Thesis, Delft University of Technology, 2016.

[13] E. Dekens, S. Engelen, R. Noomen, "A satellite swarm for radio astronomy," *Acta Astronautica*, vol. 102, pp. 321-331, 2014.

[14] R.T. Rajan, *Relative Space-Time Kinematics of an Anchorless Network*, Ph.D. Thesis, Delft University of Technology, 2016.

[15] R.T. Rajan, S. Engelen, M. Bentum, C. Verhoeven, "Orbiting low frequency array for radio astronomy," IEEE Aerospace Conference, *IEEE Aerospace Conference*, Big Sky, MT, US, March 2011.

[16] E. Dekens, *Orbit Analysis of a Low Frequency Array for Radio Astronomy*, M.S. Thesis, Delft University of Technology, 2012.

[17] S. D'Amico, O. Montenbruck, "Proximity operations of formation-flying spacecraft using an eccentricity/inclination vector separation," *Journal of Guidance, Control, and Dynamics*, vol. 29, no. 3, pp. 554-563, 2006.

[18] S. D'Amico, *Autonomous Formation Flying in Low Earth Orbit*, Ph.D. Thesis, Delft University of Technology, 2010.

[19] A.W. Koenig, S. D'Amico, "Robust and safe N-spacecraft swarming in perturbed near-circular orbits," *Journal of Guidance, Control, and Dynamics*, vol. 41, no. 8, pp. 1643-1662, 2018.

[20] T. Nie, P. Gurfil, "Lunar frozen orbits revisited," *Celestial Mechanics and Dynamical Astronomy*, vol. 130, no. 10, pp. 1-35, 2018.

Biography

***Sung-Hoon Mok**, born in South Korea in 1986, is a Postdoctoral Researcher in Faculty of Aerospace Engineering at Delft University of Technology. He received his BSc, MSc, and PhD degrees in 2008, 2010, 2014 at Korea Advanced Institute of Science and Technology (KAIST) in Korea. He worked as a Senior Researcher at Agency for Defense Development in Korea from 2014 to 2017. He acted as an attitude and orbit control researcher and mainly developed attitude determination and control methods for agile SAR satellites. Then he worked as a Research Assistant Professor at KAIST from 2017 to Feb. 2019. His research focused on satellite attitude guidance and mission planning for agile satellites. He (co-)authored more than 25 journal articles and conference papers. His research interests include spacecraft formation flying guidance and control, attitude determination and control, and mission planning.*

***Jian Guo**, born in China in 1976, is an Assistant Professor in Faculty of Aerospace Engineering at Delft University of Technology and the Theme Leader of Distributed Space Systems in the TU Delft Space Institute. He obtained BSc and MSc degrees in Engineering at Northwestern Polytechnical University in China and PhD in Mechanical Engineering at University of Leeds in UK. He has worked for more than 15 years on space activities since 2001 by acting as mission and system engineer for three satellites that have been launched and received national award for his contribution to the development of small satellite. He (co-)authored more than 80 journal articles and conference papers. His research interests include space system engineering, distributed space systems, and small satellites.*

***Eberhard Gill**, born in Germany in 1961, is a Full Professor and the Chair of the Space System Engineering group (SSE) and the Head of Space Engineering Department (SpE) at Delft University of Technology. He received a diploma in physics and holds a PhD degree in theoretical astrophysics at the Eberhard-Karls-University Tuebingen, Germany. He*

also holds a MSc degree in space system engineering at Delft University of Technology. He worked as a researcher at German Aerospace Center (DLR) from 1989 to 2006 and served as Co-PIs for several projects and as a PI for the PRISMA mission. He (co-)authored more than 250 journal articles and conference papers and 4 textbooks. He is a full member of the International Academy of Astronautics (IAA) and co-chaired the IAA Symposium on Small Satellites for Earth Observation in 2019. He is also a founding director of the TU Delft Space Institute since 2015. His research expertise includes orbit dynamics, distributed space systems, and space system engineering.

***Raj Thilak Rajan**, is an Assistant Professor with the faculty of electrical engineering, mathematics and computer science (EEMCS) at the Delft university of technology (TUD). Previously, he held research positions with diverse responsibilities at IMEC (Eindhoven, 2015-2018), University of Twente (Enschede, 2014), ASTRON (Dwingeloo, 2008-2014), CERN (Geneva, 2007-2008), Politenico di Bari (Bari, 2007-2008), Whirlpool (Pune, 2006-2007), and TIFR-NCRA (Pune, 2005). He received his Ph.D. in 2016 from the faculty of EEMCS in TUD, for the thesis titled 'Relative space-time kinematics of an anchorless network'. He was a SSPF fellow (The Netherlands, 2019), INFN fellow (Italy, 2008), MIUR fellow (Italy, 2007-2008), TIFR-VSRP fellow (India, 2005), and is an alumnus of the SSP2019 program from the international space university (ISU). Raj holds 40+ peer-reviewed publications, with first-author contributions in the fields of signal processing, aerospace, radio astronomy, nuclear physics, and sensor networks. He is a member of the IEEE signal processing, and IEEE aerospace and electronic system societies, and a reviewer for various related publications. His research interests lie in statistical inference and machine learning, with applications to distributed and autonomous sensor systems e.g., satellite swarms.*